Efficient Finite Element Analysis/Computational Fluid Dynamics Thermal Coupling for Engineering Applications

Zixiang Sun

John W. Chew

Nicholas J. Hills

Konstantin N. Volkov

Thermo-Fluid Systems UTC,
School of Engineering,
University of Surrey, Guildford,
Surrey, GU2 7XH, UK

Christopher J. Barnes
Rolls-Royce plc,
P.O. Box 31,
Derby, DE24 8BJ, UK

An efficient finite element analysis/computational fluid dynamics (FEA/CFD) thermal coupling technique has been developed and demonstrated. The thermal coupling is achieved by an iterative procedure between FEA and CFD calculations. Communication between FEA and CFD calculations ensures continuity of temperature and heat flux. In the procedure, the FEA simulation is treated as unsteady for a given transient cycle. To speed up the thermal coupling, steady CFD calculations are employed, considering that fluid flow time scales are much shorter than those for the solid heat conduction and therefore the influence of unsteadiness in fluid regions is negligible. To facilitate the thermal coupling, the procedure is designed to allow a set of CFD models to be defined at key time points/intervals in the transient cycle and to be invoked during the coupling process at specified time points. To further enhance computational efficiency, a "frozen flow" or "energy equation only" coupling option was also developed, where only the energy equation is solved, while the flow is frozen in CFD simulation during the thermal coupling process for specified time intervals. This option has proven very useful in practice, as the flow is found to be unaffected by the thermal boundary conditions over certain time intervals. The FEA solver employed is an in-house code, and the coupling has been implemented for two different CFD solvers: a commercial code and an in-house code. Test cases include an industrial low pressure (LP) turbine and a high pressure (HP) compressor, with CFD modeling of the LP turbine disk cavity and the HP compressor drive cone cavity flows, respectively. Good agreement of wall temperatures with the industrial rig test data was observed. It is shown that the coupled solutions can be obtained in sufficiently short turn-around times (typically within a week) for use in design. [DOI: 10.1115/1.3147105]

1 Introduction

To assist engine design, accurate and quick prediction of component metal temperature is one of the key issues. Traditionally in industry, finite element analysis is routinely used to predict metal temperatures with the thermal boundary conditions provided by thermocouple measurements and/or empirical correlations. The practice is still widely used in industry today. However, the limitation of this practice is obvious. Its effectiveness is subject to availability and applicability of the current database and correlations for a new design.

With rapid progress of computational fluid dynamics (CFD) capability and computer power, CFD has proven to be a useful tool to assist and to improve the metal temperature prediction. There are basically three types of approaches in using CFD solutions for solid/fluid heat transfer calculations. One is generally called "conjugate heat transfer analysis," the second "noncoupled FEA/CFD procedure" and the third one "coupled FEA/CFD analysis." These are hereafter referred to as conjugate analysis, noncoupled procedure, and coupled analysis, respectively.

In conjugate analysis, the solid/fluid heat transfer calculation may be realized by expanding the CFD capability to include heat conduction calculation in solid regions neighboring the fluids. Examples of such expanded CFD solvers for the conjugate analysis are NASA GLENN-HT code by Rigby and Lepicovsky [1], and Aachen's CHTFLOW solver by Bohn et al. [2]. A number of papers have been published showing application of the conjugate analysis for engine component temperature predictions, such as a real turbine rotor-stator system simulation by Okita and Yamawaki [3] and Okita [4] in 2002 and 2006, respectively, a blade film cooling prediction by Bohn et al. [5] in 2003, and an internally cooled turbine blade application by Kusterer et al. [6] in 2004. It was found that the applications of the conjugate analysis were limited to steady and simple transient calculations. Generally speaking, a CFD simulation is expensive. This would be especially true for a time accurate calculation of a flight cycle, as a relatively very small time step has to be used to resolve the flow unsteadiness. Therefore, the computational cost of performing a transient conjugate flight cycle analysis with an unsteady CFD solution is prohibitive.

Noncoupled procedures alleviate the CFD cost, where only a limited number of steady CFD calculations are performed at key engine operating conditions to produce a set of CFD based correlations, which eventually provide the necessary thermal boundary conditions for the traditional FEA calculation. Examples are two turbine disk cavity applications by Lewis and Provins [7] in 2004 and Alizadeh et al. [8] in 2007. However, successful application of the noncoupled procedure is very much dependent on users' experience and expertise, such as boundary segment partitioning for the discrete correlations and scaling of the correlations between the engine operating conditions.

Coupled FEA/CFD analysis is an alternative technique, where separate FEA and CFD codes are used for solid and fluid regions, respectively, with a smooth exchange of information between the two codes to ensure continuity of temperature and heat flux. The

Contributed by the International Gas Turbine Institute of ASME for publication in the JOURNAL OF TURBOMACHINERY. Manuscript received August 26, 2008; final manuscript received February 11, 2009; published online April 5, 2010. Review conducted by David Wisler. Paper presented at the ASME Turbo Expo 2008: Land, Sea and Air (GT2008), Berlin, Germany, June 9–13, 2008.

main merit of the approach is to enable users to take full advantages of both CFD and FEA capabilities. Further integration of the stress analysis can be easily realized with the FEA solver, which is equally important to designing a software package. There are a variety of approaches in implementing the coupled FEA/CFD analysis. For instance, in 1992 Heselhaus et al. [9] demonstrated a 3D FEA to 3D CFD coupling procedure for cooled turbine blade application. In a later time, Li and Kassab [10] described a coupled finite-volume method/boundary element method (FVM/BEM) approach with application to turbine blade calculation in 1994. Bohn et al. [11] reported their coupled procedure for film-cooled turbine blade applications in 1995. Recently, Illingworth et al. [12] reported a well established procedure coupling an in-house FEA code to a commercial CFD code, and successfully applied the procedure to turbine disk cavity calculations for flight cycle simulations. This followed work on steady state coupling by Mirzamoghadam and Xiao [13] and Verdicchio et al. [14].

Extensions to the work of Illingworth et al. and validations are reported in this paper. The methods employed are described in Sec. 2. Validations, including comparison with engine data, are given in Sec. 3, and conclusions are summarized in Sec. 4.

2 Modeling Methods

In the engine cycle models, the FEA calculation must be unsteady to reproduce the relatively slow response of metal heat conduction to a change in operating conditions over a given transient flight cycle. Compared with this, the fluid flow time scales are much shorter, as they are determined by the fast convection of the flow. As a result, the influence of unsteadiness of fluid flow is expected to be negligible, and steady CFD calculations may be employed. In other words the flow may be assumed to adjust instantaneously to changes in the flow boundary conditions, as the time taken for such adjustments is much smaller than other time scales for the problem considered. This saves considerable computing time for a FEA/CFD thermal coupling calculation, as it avoids expensive unsteady CFD simulation in fluid regions and allows much larger time steps for unsteady FEA simulation of the metal heat conduction in solid regions, which means fewer time steps are needed to resolve a given transient cycle. Further approximation is usually involved in modeling engine accelerations or decelerations when the engine speed is changing. This is further discussed below.

Within the FEA models, one or more local CFD boundary domains can be set up as required. They may cover part or the whole FEA model boundary. The procedure provides coupling capability for the neighboring CFD/FEA boundaries, while the rest of FEA model is still simulated using conventional thermal boundary conditions provided by thermocouple measurements and/or empirical correlations. This practice ensures great flexibility and choice for users.

The coupling is realized through an iterative loop between the FEA and CFD simulations, with communications ensuring continuity of temperature and heat flux across the coupled boundaries between the FEA and CFD models. Convergence of the thermal coupling at a thermal time point is recognized when the difference of coupled wall temperature between two adjacent successive thermal coupling iterations is reduced to a required tolerance. In the coupling process, intermediate individual FEA and CFD solutions are obtained in turn with dynamically updated boundary conditions. On coupling walls, the temperature distributions obtained in FEA simulations are used to define temperature boundary conditions for CFD models, and the heat flux distributions obtained in CFD simulations are used to define heat flux boundary conditions for the FEA model. Convergence of the individual FEA and CFD solutions is recognized when their governing equations' residuals are reduced to a required tolerance. To avoid exceptional dead lock of the individual CFD simulations, appropriate maximum numbers of iterations are assigned for each CFD model. The practice is implemented in a similar way to that for ordinary standalone CFD calculations.

To facilitate the thermal coupling, the coupling procedure is designed to allow a set of CFD models to be defined at key time points/conditions in the transient cycle to represent "steady" operating conditions, such as idle, maximum take-off (MTO), and cruise conditions. The points and the time intervals between the points are called ramp points and ramps, respectively, in a transient cycle definition (examples are given later in Sec. 3). The so-called environment parameters, such as rotational speed and mass flow rates, are stored at the ramp points. Between the ramp points, linear distributions of the environment parameters are generally assumed.

For a steady flight condition the environment parameters of the two ramp points will be identical, but metal and internal air system temperatures may change. The cycle definition provides necessary operating conditions for the CFD models. During a thermal coupling process, the corresponding CFD models are to be invoked at specified ramp points. For a ramp representing a steady flight condition, such as idle, maximum take-off (MTO), and cruise conditions, an intermediate individual CFD solution is obtained by solving the corresponding CFD model, which is then coupled with the unsteady FEA simulation.

For those ramps representing "unsteady" flight conditions, such as engine acceleration and deceleration, the CFD solution is estimated, as a further approximation, by a linear interpolation operation from the corresponding two CFD models for the neighboring steady operating conditions defined at the two end points of that ramp. In this case, the thermal boundary conditions corresponding to the time step are applied simultaneously to those two CFD models and consequently solved. The two CFD solutions are then linearly interpolated with respect to time to produce a heat transfer estimation for the time step, which is eventually used to couple the unsteady FEA simulation. This approximation is consistent with traditional modeling techniques, which do not attempt to resolve the flow variations fully during such rapid changes. Provided the accelerations and decelerations are fast enough, compared with the component temperature changes, the approximation is fully justified.

To assist the CFD calculations in the thermal coupling, primary initial solution for each CFD model was prepared in advance, assuming that all walls of the CFD domain were adiabatic. The operating conditions for those initial adiabatic CFD solutions, such as rotational speed and mass flow rates where appropriate, are provided by the cycle definition. During the thermal coupling, an intermediate CFD solution at a time step is obtained with the dynamically updated boundary conditions. The latest CFD solution obtained is then always used as initial flow field for the next time step. It can be expected that a change between CFD solutions at two neighboring successive thermal time steps should be small and gradual. Hence, fewer iterations are needed for an intermediate individual CFD solution.

Unless explicitly specified in the coupling process, the default starting point of a transient coupling is set to be a standstill condition, where an isothermal state can be assumed. The procedure has already been used as a design tool, and a number of tutorials and best practice have been established. For further details of the procedure, readers are referred to the publication by Illingworth et al.

The coupling procedure is controlled by a "plugin" (SC89) to the SC03 FEA code. SC03 is fully automated. SC89 was originally implemented to couple SC03 FEA to the commercial FLUENT CFD code [15]. It has now been extended to allow coupling with an in-house CFD code HYDRA. HYDRA was developed by Rolls-Royce plc and researcher partners [16]. It is an unstructured hybrid CFD code using the finite-volume method and an edge-based data formulation. The solver uses an explicit time-marching technique based on a five-step Runge–Kutta procedure. Convergence

is accelerated by the use of multigrid techniques and by Jacobi preconditioning for high speed flows, together with a separate low Mach number preconditioning option for low speed flows. Parallel computation is implemented using the Oplus library [17,18]. Thus the methods used in HYDRA differ significantly from those used in earlier studies which employed the pressure correction algorithm in FLUENT. The motivation for using HYDRA includes commonality with CFD software for turbomachinery applications, as discussed by Chew and Hills [19].

A CFD solution is normally obtained by solving all the governing equations of fluid flow and heat transfer. This type of CFD solution is here referred to as the "full equations" option in the present paper. An alternative to the full equations option is so-called energy equation only option, where the energy equation is solved while the flow field is frozen during the coupling process. Recomputation of the continuity and momentum equations is therefore bypassed, which can produce extra saving in computational cost. Obviously, the energy equation only option is a further approximation aimed at faster coupling performance. The energy equation only option has proven very useful in some cases. It has long been recognized that there are situations where fluid properties are essentially independent of temperature and the flow energy equation has no influence on the flow field. In this case, the flow energy equation is linear in temperature. Chew et al. [20] made use of this in their coupled CFD/FEA thermal solution for a turbine blade. In the present work an energy equation only option has been developed in HYDRA and implemented in the coupling plugin SC89. This and FLUENT have been used to explore the use of the "frozen flow" option for further accelerating coupled simulations for internal air system applications.

The energy equation only option also adopts the steady flow assumption and is implemented in a similar way to a full equations solution. Under the present multiple CFD model arrangement, the density, pressure, and velocity of all CFD models are kept unchanged during the thermal coupling. Their magnitudes are all from the prepared initial flow solutions. For a ramp representing steady flight conditions, such as idle, MTO, and cruise conditions, the energy equation only solution is obtained by solving the corresponding CFD model. For a ramp representing unsteady flight conditions, such as engine accelerations and decelerations, the energy equation only solution is obtained, as a further approximation, by a linear interpolation of the corresponding two energy equation only solutions at the two end points of that ramp with respect to time. In this case, the thermal boundary conditions corresponding to the time step are applied simultaneously to those two CFD models and consequently solved with the energy equation only facility. The energy equation only option in HYDRA was validated against solutions of the full equations for a number of test cases. Good agreement was obtained. The energy equation was solved using the same techniques as for the fluid flow solution. This is not optimal for a linear equation, but was convenient for these initial evaluations.

3 Thermal Coupling Validation

Four test cases, 2D and 3D model rotor-stator examples, plus an engine low pressure (LP) turbine cavity, and a high pressure (HP) compressor drive cone cavity were chosen for the coupling testing. Both the energy equation only and full equation CFD solutions were used in the thermal coupling. All CFD calculations were performed with the k-ε turbulence model and standard wall functions. The results obtained with HYDRA and FLUENT CFD codes were compared with available thermocouple measurements for the engine test cases.

3.1 2D Rotor-Stator Example (2D FEA/2D CFD Coupling). The FEA and CFD domains for the 2D rotor-stator example are shown in Fig. 1. It can be seen that the geometry of the FEA/CFD models simply consists of a rotor and a stator, forming a cavity with an axial inflow at inner radius along shaft and a radial outflow at outer radius. The whole geometry is strictly axisymmetric. Three key dimensions are also shown in Fig. 1. The ratio between the inner and outer radii of the cavity is $r_o/r_i=1.5$. The inner radius of the stator r_s is equal to $r_s=1.005r_i$. Consequently, the narrow radial gap between inner radii of the rotor and stator at inlet is $(r_s-r_i)=0.005r_i$. The hydraulic diameter dh at inlet is equal to $d_h=4*\text{area}/\text{wetted-perimeter}=0.01r_i$. The width of the cavity s is equal to $s=0.125r_i$. The angular speed of the rotor Ω is 800 rad/s. The axial inflow Reynolds number $\text{Re}_{\text{bulk}}=\rho U_{\text{bulk}}d_h/\mu$ and the rotational Reynolds number $\text{Re}_\Omega=\rho r_o^2\Omega/\mu$ based on the inflow condition are 3.42×10^4 and 9.54×10^6, respectively. These justify the use of turbulent flow simulation. The mesh employed is also shown in Fig. 1. The total number of grid nodes is 5265. The mesh was generated following previous experience. For this mesh, the dimensionless wall distance y^+ obtained is between 20 and 120, within the recommended range for use of the wall function. A mesh independence investigation also showed that the mesh is reasonable. The CFD model provides boundary conditions for the inner rotor and stator faces labeled as coupling wall. Conventional boundary conditions are specified on the other faces labeled as noncoupling wall, using a specified gas temperature and heat transfer coefficients obtained from a correlation for rotating disk heat transfer.

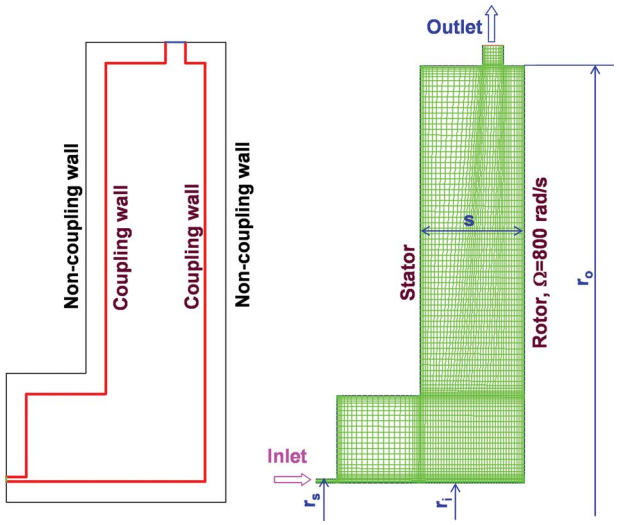

Fig. 1 2D rotor-stator FEA and CFD models

The transient thermal cycle simulated is given in terms of rotor angular speed versus time in Fig. 2. In fact, the rotor angular speed is one of the parameters needed to provide a time series of operating information to run a FEA/CFD coupling. The other necessary parameters for this FEA/CFD coupling are mass flow rate, temperature, and operating pressure. For clarity, only the rotor angular speed is used here to indicate the transient cycle. As shown in Fig. 2, the rotor starts from standstill and accelerates within 60 s to its maximum speed at 800 rad/s, then keeps steady until 210 s to stabilize the system.

Two operating conditions and three ramp points are defined to facilitate the FEA/CFD coupling, as shown in Fig. 2. Conditions 1 and 2 designate standstill and maximum loading, respectively. Ramp points 1–3 correspond to the starting point at standstill condition 1 (time $t=0$), the end point of acceleration at time $t=60$ s and finish point of the stabilization period at time $t=210$ s. In the coupling procedure, the time step is always initially set to be $\frac{1}{4}$ of the time interval between two ramp points. The time step will be reduced if a given thermal time stepping accuracy limit is exceeded. The thermal time stepping accuracy was set to 2 K in the present test case. For a typical engine cycle, the thermal time stepping accuracy is generally set to be 5 K or 10 K in industrial

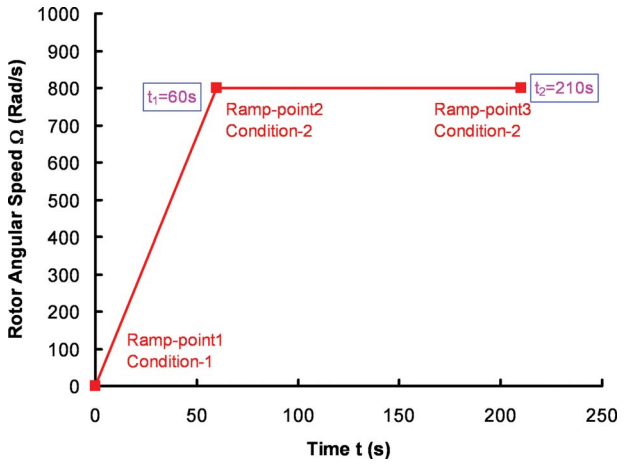

Fig. 2 Cycle definition for 2D rotor-stator FEA/CFD thermal coupling

practice. For the present thermal coupling, a smaller magnitude of thermal time stepping accuracy was chosen to ensure sufficient accuracy in this initial test case. The thermal time stepping accuracy works in the following way. For each FEA node, the values of temperature obtained at the current time point and the last two time points, i.e., three adjacent successive intermediate coupling solutions, are used to generate piecewise linear and parabolic curve fits for the temperature history. When the maximum difference of temperature between the two curve fits is larger than a given time stepping accuracy, the time step will be reduced. The assessment of time stepping accuracy is performed over the whole FEA domain and the adjustment of time step is fully automated. It has been shown that using the time stepping accuracy instead of the maximum temperature increment to control the time step adjustment improves overall performance of transient thermal simulation with better accuracy and robustness. The convergence criterion of the thermal coupling was set to 0.5 K in the present test case from the experience of earlier studies. Typically, the magnitude of this parameter is recommended to be equal to or less than $\frac{1}{4}$ of the magnitude of thermal time stepping accuracy. As described before, the convergence criterion for the thermal coupling denotes the maximum wall temperature difference allowed between two adjacent successive intermediate coupling solutions at a time point in the FEA/CFD coupling loop. The maximum number of iterations for individual CFD solutions was assigned to 200, following earlier experience and some numerical experiments.

An initial CFD solution was prepared in advance for Condition-2 assuming, at this stage, that all the walls of the CFD model are adiabatic. A view of the stream function contours of the initial flow solution is shown in Fig. 3. It can be seen that a jet flow from the inlet travels axially toward the rotor in the inner radius. Along the rotor wall the fluid is centrifuged radially-outwards. A portion of the flow leaves the domain through the outlet at the outer radius, and part of it moves back radially along the stator side to the inner radius to meet the requirement of continuity. Consequently a big circulation is formed in the domain, which is the major feature of the flow. In the inner corner formed by the stator, there exists another smaller circulation, induced by the jet flow and the major circulation. The flow is mainly controlled by the rotation and through-flow. Buoyancy effects are less important. Also in Fig. 3, ten monitoring points distributed on the cavity inner walls for temperature time history are shown for reference.

Both energy equation only and full equation FEA/CFD coupling calculations were conducted using the HYDRA and FLUENT codes. The wall temperature histories obtained at two typical monitoring points R3 and S3 at the middle radius are given in Fig.

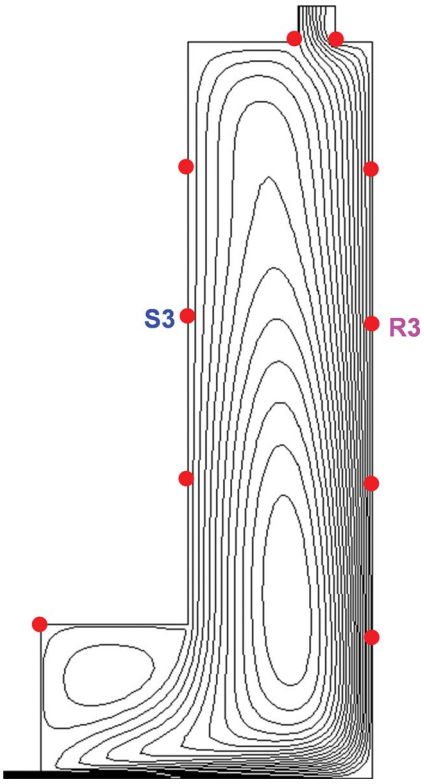

Fig. 3 Initial adiabatic CFD solution for 2D rotor-stator FEA/CFD thermal coupling

4. The dash and solid lines indicate the results obtained using HYDRA with the energy equation only option on the rotor and stator walls, respectively. The circle and square symbols designate their corresponding counterparts obtained using HYDRA with the full equations option. The plus and cross signs denote those obtained using FLUENT with the energy equation only option. To avoid further overlay of the plots, the coupling results obtained using FLUENT with the full equations option are not presented in the figures. Agreement between all these results, obtained using either the energy equation only or the full equations options in either HYDRA or FLUENT is very good. Comparisons between solutions at other monitoring points show equally good agreement.

A view of temperature contours at time $t=210$ s, i.e., at the end of the thermal coupling, obtained using HYDRA with the energy equation only option is shown in Fig. 5. Such data can be further used in thermal stress analysis and displacement calculation when necessary. A comparison of wall temperature distributions be-

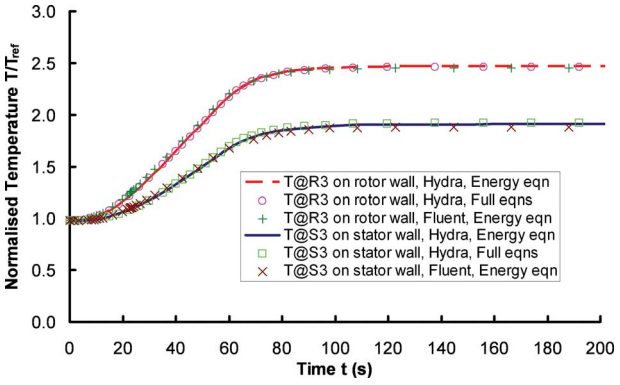

Fig. 4 Comparison of wall temperature histories for 2D rotor-stator FEA/CFD thermal coupling

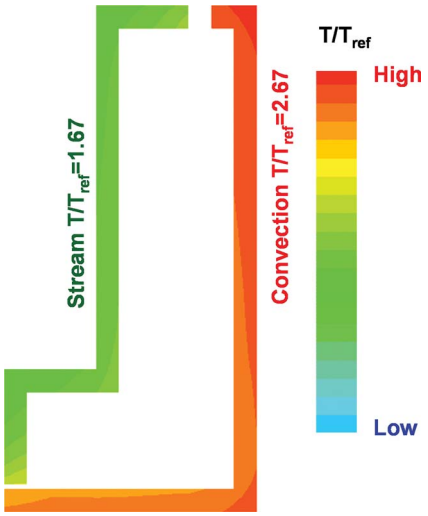

Fig. 5 Metal temperature contours at time t=210 s for 2D rotor-stator FEA/CFD thermal coupling

tween the solutions obtained with different coupling options is given in Fig. 6. The dash and solid lines represent the results obtained using HYDRA with the energy equation only option on the rotor and stator walls, respectively. The symbols designate their corresponding counterparts obtained either using HYDRA with the full equations option or FLUENT with the energy equation only option. It can be seen again that agreement between these solutions is very good.

A further coupling calculation using HYDRA with the maximum number of iterations reduced from 200 to 50 for individual CFD solutions was also conducted. Similar good results were obtained. Further discussion of the influence of CFD solution convergence on the thermal coupling is presented later in Sec. 4.

3.2 3D Rotor-Stator Example (2D FEA/3D CFD Coupling). The 3D rotor-stator example is a variation in the aforementioned 2D model. The FEA model and the transient cycle definition remain the same as in 2D example, except that the 3D rotor-stator sector CFD model shown in Fig. 7 is employed to replace the corresponding 2D axisymmetric one. Hence, the resultant thermal coupling calculations are a 2D axisymmetric FEA model coupled with a 3D sector CFD model. To accommodate the change, a routine to map information exchange between a 2D axisymmetric FEA model and a 3D sector CFD model was also

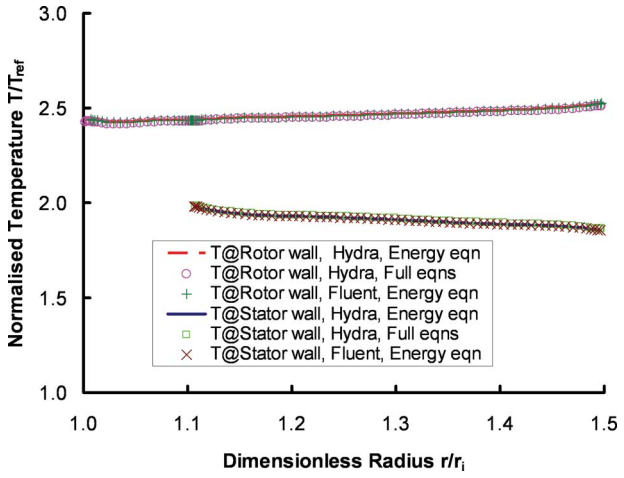

Fig. 6 Wall temperature distributions at time t=210 s for 2D rotor-stator FEA/CFD thermal coupling

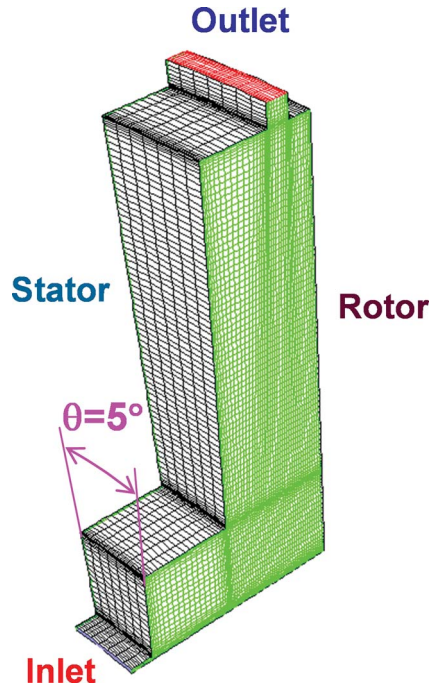

Fig. 7 3D rotor-stator sector CFD model

invoked. On coupling walls, the mapping routine enables the 3D CFD model to pass circumferentially-averaged wall heat flux distributions to the 2D FEA model, and the 2D FEA model to expand the 2D wall temperature profiles obtained into 3D ones (assuming uniform distribution in the circumferential direction), which can applied to 3D CFD models.

Only the HYDRA CFD code was used for this test case. As for the 2D example, excellent agreement was obtained between fully coupled and energy equation only coupled solutions. These were also in agreement with the 2D solutions.

3.3 Engine Turbine Example (2D FEA/2D CFD Coupling). A 4 stage LP turbine disk cavity was chosen for further testing. This industrial engine test case is well established with a set of thermocouple data available for comparison. The geometry of the FEA and CFD models are shown in Fig. 8. The CFD domain is in the left side of the figure, bounded by the IP turbine disk rear face, the first two LP turbine disks, the front face of the third IP turbine disk and the IP and LP turbine shafts, and FEA/CFD thermal coupling takes place through these boundaries. Both FEA and CFD models are axisymmetric. Three key dimensions are also shown in this figure. The inner radius of the cavity along shaft is denoted as r_i. The inner radii of the intermediate pressure (IP) turbine shaft and LP turbine disk bore are designated as r_s and r_b, with $r_s \approx 1.13 r_i$ and $r_b \approx 3.54 r_i$, respectively. The hydraulic diameter of the inner inlet along the shaft is $d_h \approx 0.25 r_i$.

The simulated transient cycle in terms of the LP turbine disk angular speed Ω versus time is given in Fig. 9. It can be seen that

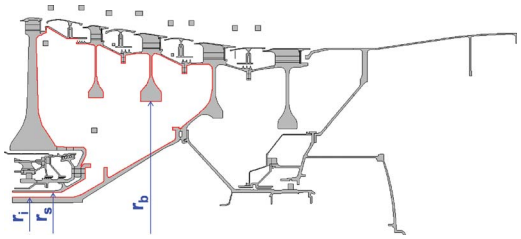

Fig. 8 FEA and CFD models for a LP turbine cavity

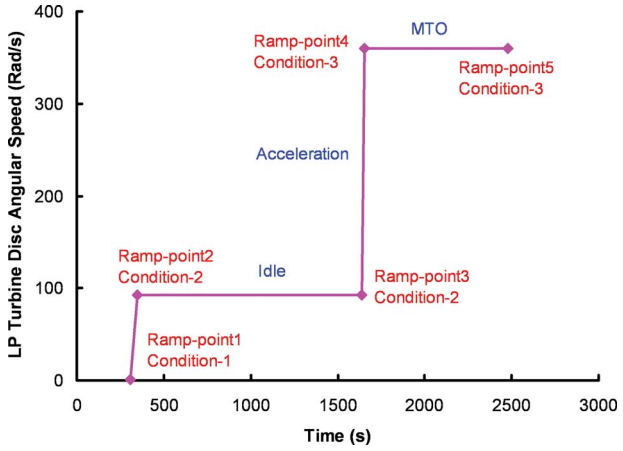

Fig. 9 Transient thermal cycle for the LP turbine cavity

the transient cycle covers a typical range of operating conditions from idle to maximum take-off. Based on the flow at the inner inlet along the shaft and the LP turbine disk angular speed, the axial inflow Reynolds number $\mathrm{Re}_{\mathrm{bulk}}=\rho U_{\mathrm{bulk}} d_h/\mu$ and the rotational Reynolds number $\mathrm{Re}_{\Omega}=\rho r_b^2\Omega/\mu$ are 7.07×10^4 and 2.97×10^5, respectively, for idle condition, and 2.39×10^5 and 2.04×10^6, respectively, for MTO condition. Hence, the assumption of turbulent flow is justified.

Two CFD models, one for idle and the other for maximum take-off, were defined to facilitate the FEA/CFD coupling. The mesh sizes used for idle and maximum take-off conditions were 38,378 and 67,310 nodes, respectively, which were determined following previous experience and best practice guidelines. The dimensionless wall distance y^+ obtained is between 15 and 100, within the recommended range for use of the standard wall function. A whole view of the mesh used for the idle condition is shown in Fig. 10, with a close-up at the upper left corner of the CFD domain for further examination. The boundary conditions for the CFD model are also illustrated in Fig. 10. It has two mass flow inlets and four outlets. Further details of the FEA and CFD models follow industrial practice. The environment parameters defined in the transient cycle, such as angular rotational speed and mass flow rate, are passed to the corresponding walls, inlets, and outlets through the plugin SC89 when appropriate. Conventional thermal boundary conditions are applied on the remaining boundaries for the FEA model.

With the above settings, two primary initial CFD solutions, one for idle and the other for the maximum take-off, assuming adiabatic walls were prepared in advance, as shown in Fig. 11. It can

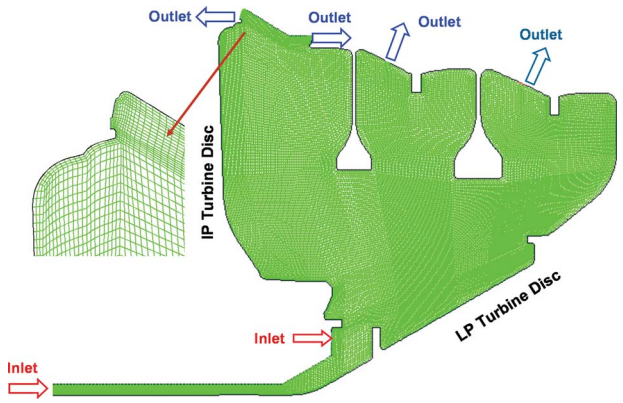

Fig. 10 Typical mesh of the CFD model for the LP turbine cavity

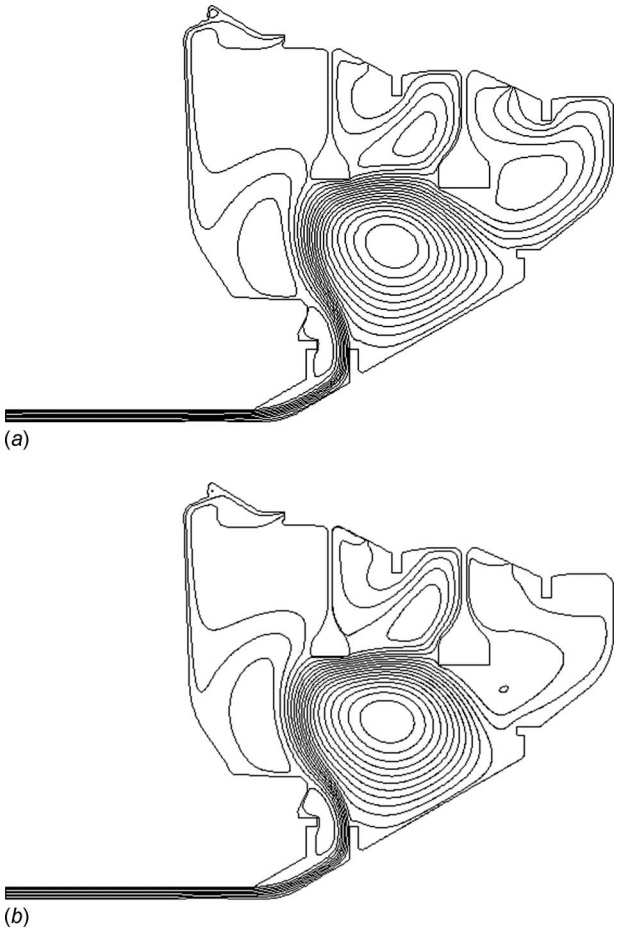

Fig. 11 Two initial adiabatic CFD solutions for the LP turbine cavity; (*a*) idle, (*b*) MTO

be seen that the jet flow from the inner inlet along the shaft travels axially and is then directed radially into the cavity by the LP turbine disk and baffle. Inside the cavity, the flow is dominated by the effect of wall rotations. Consequently, several vortices are formed. Buoyancy effects are weak in this flow. By comparing the flow patterns obtained between the idle and maximum take-off conditions, a degree of similarity in flow patterns can be identified between those two very different operating conditions. As the primary focus of this paper is on the thermal coupling methodology and validations, no further analysis of the flow solutions was pursued.

In the transient thermal coupling, the thermal time stepping accuracy to control the adjustment of the thermal time step was set to be 5 K, and the convergence criterion of thermal coupling in terms of maximum metal temperature difference allowed between two successive coupling iterations was set to be 1 K. These values are typical for engine applications. For individual HYDRA CFD solutions, the maximum number of iterations per thermal time step was assigned to be 300 and 60 for the idle and the maximum take-off CFD models, respectively, following earlier experience and some numerical experiments. Figure 12 shows the temperature histories at three monitoring points, obtained using both energy equation only and full equations options. The metal temperature contours obtained at the end of the thermal coupling transient cycle are also given in this figure for an overall picture of temperature distribution at $t=2477$ s. For comparison, the thermocouple data provided by Rolls-Royce plc were also plotted, together with coupling results using the FLUENT CFD code. For FLUENT solutions, 200 iterations were assigned for each CFD calculation. In Fig. 12, the dash and solid lines indicate the results

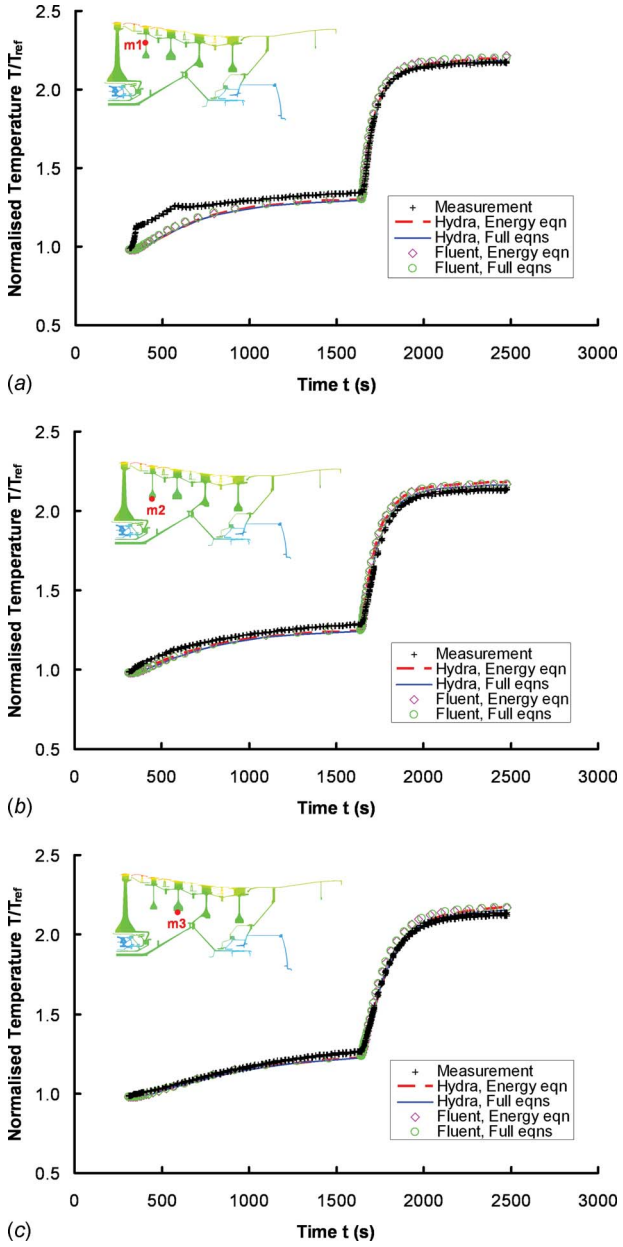

Fig. 12 Monitored temperature histories for the LP turbine cavity

obtained using HYDRA CFD solutions with energy equation only and full equations options, respectively. The black plus signs denote the Rolls-Royce thermocouple measurements. The diamond and circle symbols designate their corresponding counterparts obtained using FLUENT. It can be seen that agreement between the thermal coupling results using energy equation only and full equations options with the HYDRA and FLUENT codes is very good. The agreement between the thermal coupling predictions and Rolls-Royce measurements is satisfactory, which is generally within the measurement uncertainty. The behavior of the thermocouple measurements at the start of the transient cycle in Fig. 12(*a*) is not understood.

3.4 Industrial Compressor Example (2D FEA/2D CFD Coupling). To further validate the energy equation only option, an industrial high pressure compressor drive cone cavity was chosen for additional testing. This engine test case is also well established with a set of thermocouple measurements available for comparison. The geometry of the FEA model is shown in Fig. 13. The

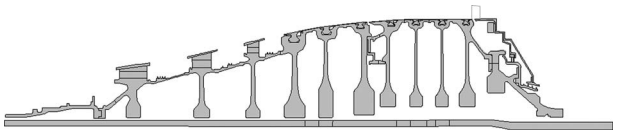

Fig. 13 FEA and CFD models for a HP compressor drive cone cavity

CFD domain is in the upper right corner of the figure, which includes a section of main annular passage of compressor at outer radius. Both FEA and CFD models are axisymmetric. The ratio between inner and outer radii of the drive cone is equal to $r_o/r_i \approx 1.50$.

The simulated transient cycle in terms of the drive cone angular speed Ω versus time is given in Fig. 14. It covers a typical range of operating conditions from standstill to idle and MTO. Based on the flow at the outer inlet of main annular path and the drive cone angular speed, the axial inflow Reynolds number $\mathrm{Re}_{\mathrm{bulk}} = \rho U_{\mathrm{bulk}} d_h / \mu$ and the rotational Reynolds number $\mathrm{Re}_\Omega = \rho r_o^2 \Omega / \mu$ are 3.53×10^5 and 4.32×10^6, respectively, for the idle condition, and 1.26×10^6 and 2.27×10^7, respectively, for MTO condition. The radial inflow Reynolds number $\mathrm{Re}_{\mathrm{bulk}} = \rho U_{\mathrm{bulk}} d_h / \mu$ based on the flow entering the cavity from the main annular passage of compressor are 2.10×10^3 and 1.30×10^4 for the idle and MTO conditions, respectively. Hence, the assumption of turbulent flow is again justified.

For this engine test case, only the coupling simulation using the FLUENT energy equation only solutions was performed. To facilitate the FEA/CFD coupling, two CFD models, one for idle and the other for maximum take-off, were defined, as shown in Fig. 15. There is one inlet and three outlets. The mesh sizes used for the idle and maximum take-off conditions were 14,589 and 32,756 nodes, respectively. The meshes were generated following previous experience and best practice guidelines. The dimensionless wall distance y^+ is between 20 and 200, within the recommended range for use of the standard wall function. For reference, the initial flow solutions assuming adiabatic walls prepared in advance for the coupling simulation are also shown in Fig. 15. It can be seen the cooling air flow enters the cavity from the main annular path of the compressor and travels radially-inwards to the inner radius along the stator wall. Part of the flow leaves the cavity through the two outlets on the stator wall in the inner region. In addition to this, recirculation flow is caused in the cavity by the rotational effects of the HP compressor drive cone. Due to the complexity of the geometry of the cavity, several vortices are formed. As in earlier examples, buoyancy effects are weak in this

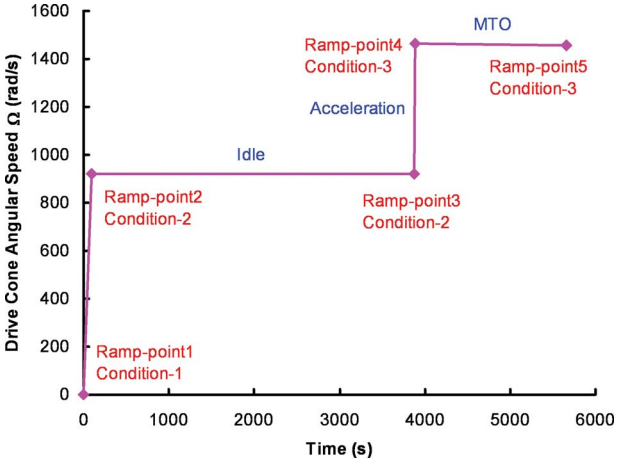

Fig. 14 Transient thermal cycle for the HP compressor drive cone cavity

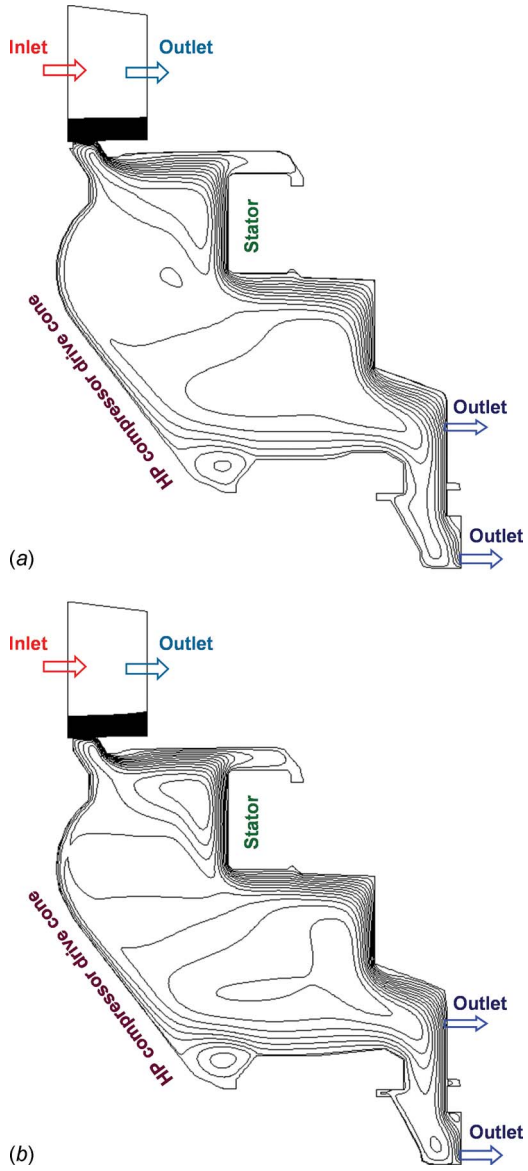

Fig. 15 Initial adiabatic CFD solutions for the HP compressor drive cone cavity; (*a*) idle, (*b*) MTO

flow. By comparing the flow patterns obtained between the idle and maximum take-off conditions, a degree of similarity in flow patterns can be again observed between these two very different operating conditions. As the primary focus of this paper is on the thermal coupling methodology and validations, no further analysis of flow solutions was performed.

In the transient thermal coupling, the thermal time stepping accuracy was set to be 10 K, and the convergence criterion for metal temperature accuracy was set to be 2 K. A major consideration in choosing the bigger magnitudes of tolerance is the computational cost. It can be seen from Fig. 14 that the present coupling simulation has to cover a much longer time span of the engine transient cycle. In addition, previous experience shows that bigger magnitudes of tolerance may be needed for thermal coupling applications with greater complexity of the geometry and larger FEA/CFD models. The magnitudes of tolerance chosen for the present test case are still within the recommended range for a typical engine application, and no noticeable compromise in accuracy of the thermal coupling solution was observed. For individual FLUENT CFD solutions, the maximum number of iterations per thermal time step was assigned to be 200 for both the idle and

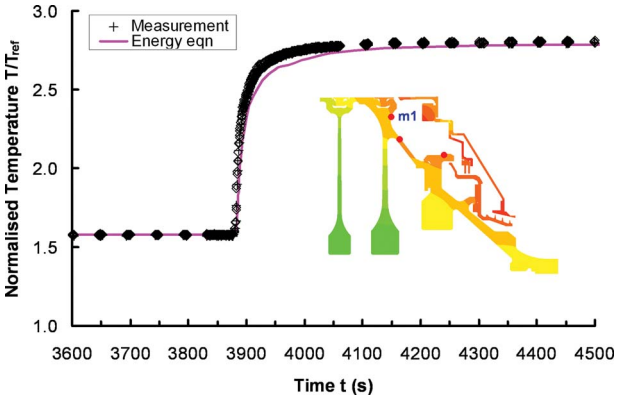

Fig. 16 Monitored temperature histories for the HP compressor drive cone cavity

the maximum take-off CFD models. A typical monitored temperature history obtained at point m1 is shown in Fig. 16, together with the thermocouple data from Rolls-Royce plc. A partial view of the metal temperature contours obtained at the end of the thermal coupling transient cycle $t=5658$ s is also given in the figure, together with the three monitoring points. The solid line indicates the thermal coupling results. The plus symbols denote the thermocouple measurements. It can be seen that agreement is reasonably good. Similarly good agreement was observed at the other two monitoring points.

4 Computational Cost

The computing time consumed for two thermal coupling calculations are given in terms of wall-clock time in Table 1. It can be seen that all coupling simulations finished within 25 h. The timings were obtained on a PC-cluster cluster node with a 2.4 GHz Xeon CPU. Timing of the initial adiabatic CFD solutions is not included in Table 1. In the four test cases reported in this paper, the initial adiabatic CFD solutions were all obtained in less than 6 h CPU time, reflecting the CFD mesh sizes all being considerably less than 100,000 mesh nodes. For medium and large thermal coupling simulations, parallel execution of the FEA/CFD coupling is available, which can help to meet the time requirement. Use of the energy equation only option can reduce the computing time, as demonstrated in Table 1. The speedup is defined as a ratio of the wall-clock time consumed between using the energy equation only option and its corresponding full equations one. It can be seen that the speedup obtained for the two test cases are 1.4 and 3.1, respectively. Obviously, it is case dependent.

It was observed in the FEA/CFD coupling simulations that FEA thermal time stepping is affected by how well individual CFD solutions are converged. In the SC03 FEA code, the thermal time stepping is automatically adjusted during the transient simulating cycle to meet a preset accuracy criterion for thermal coupling, and the whole FEA analysis is fully automated. Therefore, an additional investigation was conducted to examine the issue. The initial results showed that poor individual CFD solutions can consume more thermal time steps as the thermal coupling simulation struggles to meet the preset convergence criteria. Poor speedup and thermal coupling results can also be observed when individual CFD solutions are not sufficiently converged. In these cases, an

Table 1 Computing time for two thermal coupling test cases

Wall clock time (h)	Full eqns	Energy eqn only	Speedup
2D rotor-stator	14	10	1.4
Industrial turbine cavity	25	8	3.1

appropriate requirement of the residual accuracy or an increase in and the maximum number of iterations for individual CFD models is necessary, which usually means more computation time for each CFD simulation. After a number of test calculations, it was found that an intermediate individual CFD solution, which starts from its previous successive CFD solution with a set of updated boundary conditions, may be regarded as adequately converged when its residual levels are reduced by an order of magnitude. Use of this criterion gave significant saving in computing time. A CFD experiment prior to a thermal coupling simulation is advised to determine an optimal number of iterations for individual CFD models.

5 Conclusions

A technique for efficiently coupling finite element analysis to computational fluid dynamics (FEA/CFD) for thermal calculations is described. With the technique, a CFD model is integrated into an existing FEA system containing other specialist modeling options. This provides flexibility and choice to users. The thermal coupling is realized through an iterative procedure between FEA and CFD calculations. The FEA simulation is treated as transient and the CFD calculations are regarded as steady. Communication between FEA and CFD calculations ensures continuity of temperature and heat flux. Implementation of the technique was originally done with an in-house FEA code SC03 and a commercial CFD code FLUENT. Extension to couple with an in-house CFD code HYDRA was completed. The energy equation only option was developed to further enhance the speed of the thermal coupling.

Four thermal coupling test cases, including an industrial LP turbine cavity and a HP compressor drive cone cavity were investigated. Results obtained were compared either with those obtained with the commercial CFD code FLUENT and/or with available thermocouple measurements from Rolls-Royce plc. Good agreement was observed.

The computational time consumed for thermal coupling simulations of test cases were within 25 h in terms of wall-clock time using a PC-cluster node with a 2.4 GHz Xeon CPU. For medium and large thermal coupling simulations, parallel execution of the FEA/CFD coupling is available to meet the time requirement. Use of the energy equation only option can reduce computing time. A speedup of around 1.4–3.1 was obtained by using the energy equation only option in the thermal coupling in the present validations. To determine the optimal number of iterations for individual CFD models, a CFD experiment prior to a thermal coupling simulation is advised. Initial investigation on the issue showed a CFD solution may be regarded as adequately converged when residual levels are reduced by an order of magnitude.

As the current implementation of the energy equation only option in HYDRA uses the nonlinear CFD solver algorithm, further speedup of the coupling simulation is thought to be possible using other techniques. Further research in this area is planned.

Nomenclature

d_h = hydraulic diameter at inlet=4∗area/wetted-perimeter
$\mathrm{Re}_{\mathrm{bulk}}$ = inflow Reynolds number=$\rho U_{\mathrm{bulk}} d_h/\mu$
Re_{Ω} = rotational Reynolds number=$\rho\Omega r_o^2/\mu$ or $\rho\Omega r_b^2/\mu$
r = radius
r_b = disk bore inner radius
r_i = inner radius
r_o = outer radius
r_s = stator or IP turbine shaft radius
s = cavity width
T = temperature
T_{in} = air temperature at inlet
T_{ref} = reference temperature
T_w = wall temperature
t = time
U_{bulk} = bulk velocity at inlet
y^+ = dimensionless wall distance=$\rho(\tau_w/\rho)^{0.5} y_p/\mu$
y_p = wall distance

Greek

μ = dynamic viscosity
ρ = density
τ_w = wall shear stress
Ω = angular velocity of rotor or disk

Acknowledgment

Funding from the Department of Trade and Industry (DTI) and Rolls-Royce plc is gratefully acknowledged. The engine experimental data were supplied by Rolls-Royce plc. The research project was coordinated by Yoon K. Ho of Rolls-Royce and monitored for the DTI by Pat Ashill.

References

[1] Rigby, D. L., and Lepicovsky, J., 2001, "Conjugate Heat Transfer Analysis of Internally Cooled Configurations," ASME Paper No. GT2001-0405.
[2] Bohn, D., Kruger, U., and Kusterer, K., 2001, "Conjugate Heat Transfer: An Advanced Computational Method for the Cooling Design of Modern Gas Turbine Blades and Vanes," *Heat Transfer in Gas Turbine*, B. Sunden and M. Faghri, eds., WIT, Southampton, UK, pp. 58–108.
[3] Okita, Y., and Yamawaki, S., 2002, "Conjugate Heat Transfer Analysis of Turbine Rotor-Stator Systems," ASME Paper No. GT2002-30615.
[4] Okita, Y., 2006, "Transient Thermal and Flow Field in a Turbine Disk Rotor-Stator System," ASME Paper No. GT2006-90033.
[5] Bohn, D., Ren, J., and Kusterer, K., 2003, "Conjugate Heat Transfer Analysis for Film Cooling Configurations With Different Hole Geometries," ASME Paper No. GT2003-38369.
[6] Kusterer, K., Bohn, D., Sugimoto, T., and Tanaka, R., 2004, "Conjugate Calculations for a Film-Cooled Blade Under Different Operating Conditions," ASME Paper No. GT2004-53719.
[7] Lewis, L. V., and Provins, J. I., 2004, "A Non-Coupled CFD-FE Procedure to Evaluate Windage and Heat Transfer in Rotor-Stator Cavities," ASME Paper No. GT2004-53246.
[8] Alizadeh, S., Saunders, K., Lewis, L. V., and Provins, J., 2007, "The Use of CFD to Generate Heat Transfer Boundary Conditions for a Rotor-Stator Cavity in a Compressor Drum Thermal Model," ASME Paper No. GT2007-28333.
[9] Heselhaus, A., Vogel, D. T., and Krain, H., 1992, "Coupling of 3D-Navier-Stokes External Flow Calculations and Internal 3D-Heat Conduction Calculations for Cooled Turbine Blades," AGARD, pp. 40.1–40.9.
[10] Li, H., and Kassab, A. J., 1994, "A Coupled FVM/BEM Approach to Conjugate Heat Transfer in Turbine Blades," AIAA/ASME Sixth Joint Thermophysics Conference, Colorado Springs, CO, June 20–23, AIAA Paper No. 94-1981.
[11] Bohn, D., Bonhoff, H., Schonenborn, H., and Wihelmi, H., 1995, "Validation of a Numerical Model for the Coupled Simulation of Fluid Flow and Adiabatic Walls With Application to Film-Cooled Turbine Blades," VDI-Ber., **1186**, pp. 259–272.
[12] Illingworth, J. B., Hills, N. J., and Barnes, C. J., 2005, "3D Fluid-Solid Heat Transfer Coupling of an Aero Engine Pre-Swirl System," ASME Paper No. GT2005-68939.
[13] Mirzamoghadam, A. V., and Xiao, Z., 2002, "Flow and Heat Transfer in an Industrial Rotor-Stator Rim Sealing Cavity," ASME J. Eng. Gas Turbines Power, **124**, pp. 125–132.
[14] Verdicchio, J. A., Chew, J. W., and Hills, N. J., 2001, "Coupled Fluid/Solid Heat Transfer Computation for Turbine Discs," ASME Paper No. 2001-GT-012.
[15] FLUENT Inc., 2006, FLUENT User's Guide, http://www.FLUENT.com.
[16] Rolls-Royce plc, 2005, The HYDRA User's Guide, http://www.rolls-royce.com.
[17] Crumpton, P. I., and Giles, M. B., 2002, "Oplus FORTRAN77 Library," http://www.comlab.ox.ac.uk.
[18] Hills, N. J., 2007, "Achieving High Parallel Performance for an Unstructured Unsteady Turbomachinery CFD Code," Aeronaut. J., **111**, pp. 185–193.
[19] Chew, J. W., and Hills, N. J., 2007, "CFD for Turbomachinery Internal Air Systems," Philos. Trans. R. Soc. London, Ser. A, **365**, pp. 2587–2611.
[20] Chew, J. W., Taylor, I. J., and Bonsell, J. J., 1996, "CFD Developments for Turbine Blade Heat Transfer," IMechE Conf. Trans., **1**, pp. 51–64.